ELSEVIER

Journal of Nuclear Materials 318 (2003) 215–227

journal of nuclear materials

www.elsevier.com/locate/jnucmat

Tensile properties of 9Cr–1Mo martensitic steel irradiated with high energy protons and neutrons

J. Henry [a,*], X. Averty [b], Y. Dai [c], P. Lamagnère [a], J.P. Pizzanelli [b], J.J. Espinas [b], P. Wident [a]

[a] *CEA Saclay, SRMA, F-91 191 Gif-sur-Yvette cedex, France*
[b] *CEA Saclay, SEMI, F-91 191 Gif-sur-Yvette cedex, France*
[c] *Spallation Source Division, Paul Scherrer Institut, CH-5232 Villigen, Switzerland*

Abstract

Tensile specimens of 9Cr–1Mo martensitic steel in three metallurgical conditions (tempered, 20% cold-worked and as-quenched) were irradiated in SINQ target-3 with high energy protons and spallation neutrons at temperatures between about 130 and 310 °C to doses between 4 and 12 dpa. Tensile properties were measured mostly at room temperature but a limited number of tests were performed at 250 and 350 °C. Scanning electron microscopy observations of fracture surfaces as well as reduction of area measurements were performed in selected cases. Results of preliminary TEM investigations carried out on 3 mm discs irradiated together with the tensile specimens are also presented. Tensile properties are compared with earlier results on martensitic steels irradiated in spallation conditions as well as with tensile data obtained for the same heat of 9Cr–1Mo steel after irradiation with fission neutrons in the OSIRIS reactor. The as-quenched specimens displayed a fully brittle behaviour and SEM observations revealed an intergranular fracture mode. The irradiated cold-worked and annealed specimens showed large increases in strength as well as drastic reductions in uniform elongation up to a dose of about 10 dpa. The fracture surface appearances remained however ductile. The few specimens irradiated to higher doses (up to 12 dpa) recovered significant ductility, which is presently not understood on the basis of the available preliminary microstructural data.

1. Introduction

In 1996, the SINQ target irradiation program (STIP), an international collaboration between different laboratories from Europe, the USA and Japan was set up in order to irradiate and test various candidate structural materials for spallation neutron sources. To this end, miniature specimens were inserted inside the SINQ target-3 which was subsequently irradiated for 15 months with 570 MeV protons [1]. The specimens were thus bombarded with intense fluxes of high energy protons and neutrons, i.e. a radiation environment representative of the service conditions to which the structural materials of future spallation facilities will be submitted. Following irradiation, specimens were shipped by the middle of 2001 to the different participating laboratories where post-irradiation examination (PIE) programs were started. Compared to the specimens irradiated at low temperature (below 150 °C) at the Los Alamos National Laboratory (LANL) as part of the R&D program for the Accelerator Production of Tritium (APT) project, the irradiation temperature range for the SINQ specimens was larger, from 70 °C to above 400 °C. The obtained results in the STIP PIE programmes will therefore complement the recently published data [2,3] on different materials irradiated at LANL.

We report here on the tensile tests performed at CEA Saclay on 9Cr–1Mo specimens. Results of scanning electron microscopy (SEM) observations of fracture

* Corresponding author. Tel.: +33-1 69088508; fax: +33-1 69087130.
E-mail address: jean.henry@cea.fr (J. Henry).

0022-3115/03/$ - see front matter © 2003 Elsevier Science B.V. All rights reserved.
doi:10.1016/S0022-3115(03)00119-3

surfaces as well as preliminary transmission electron microscopy (TEM) microstructural examinations will also be presented.

2. Experimental

2.1. Materials

The chemical composition of the 9Cr–1Mo steel (EM10 grade) used in this study is given in Table 1. Plates of this material were normalised at 980 °C for 30 min, air cooled and tempered at 750 °C for 30 min, followed by air cooling. They were subsequently 20% cold-rolled to obtain 0.4 mm thick sheets. Some of these sheets were given a second temper treatment. Finally, one of the tempered sheets was normalised and quenched. Three different metallurgical conditions were obtained in this way: tempered and 20% cold-worked martensite, tempered martensite and as-quenched martensite.

Miniature tensile specimens, 0.4 mm thick and with a 5 mm gauge length were machined by spark erosion. Discs 3 mm in diameter were punched out from strips cut from the 0.4 mm thick sheets and mechanically polished down to a thickness of 100 μm. These discs were used following the irradiation to prepare thin foils suitable for TEM examinations. All specimens were then shipped to PSI where they were laser-marked and subsequently polished slightly in order to remove traces of welded material due to marking.

The tensile and TEM samples were then placed together with other samples in specimen carriers and loaded into Zircalloy-2 tubes. A total of 10 specimen rods were prepared: the EM10 specimens were located either in Rod 1, which was the first specimen rod placed in the path of the proton beam, or in Rod 10. Details concerning specimen loading and rod locations in the target can be found in [1].

2.2. Irradiation conditions

The SINQ target-3 was irradiated for 15 months and received a total proton charge of 6.8 Ah. Dpa values, as well as helium and hydrogen concentrations were calculated for each specimen in the target using the LAHET and MCNP-X codes. Gamma spectra obtained from irradiated dosimetry discs were used to adjust the calculated values, as described in [4].

Irradiation temperatures had also to be calculated for each specimen, using the ANSYS code. The calculated results were found to be in reasonably good agreement with the values measured by the 6 thermocouples inserted in three of the specimen rods [1].

The average beam intensity on the target was not constant during the 15 months of irradiation. After 13 months, during which the irradiation temperature range was 70 to about 350 °C, there was a 25% increase of the beam intensity due to changes in the main beam-line and therefore the specimen irradiation temperatures were also increased. During the last two months, the maximum irradiation temperature in the target reached 420 °C. Calculated dpa values and irradiation temperatures as well as H and He concentrations are given in Table 2.

An unfortunate incident occurred during beam-tuning following the modification in the beam-line: for a few seconds the target was hit by a focused beam with very high intensity. As a result, some of the aluminium samples melted and stuck other samples together. Another consequence is that some specimens have presumably reached high temperatures. Since the actual beam geometry during the short excursion time was not known, it was not possible to calculate the temperature histories of the samples included in the present study. Nevertheless, TEM investigations on disc samples located at positions where the calculated irradiation temperature was highest did not reveal any obvious effect of the temperature excursion on the irradiation-induced microstructures [5].

2.3. Test conditions

The irradiated specimens were tested using an Instron machine equipped with a 1 kN load cell. For testing the miniature specimens, special grips were used which allowed to apply the load under the specimen shoulders. Tests were performed in air at a strain rate of 3×10^{-4} s^{-1}. Since irradiation temperatures were different for all specimens, it was agreed between the different STIP partners that in addition to room temperature tests, some samples would be tested at 250 and possibly 350 °C. Test temperatures are given in Table 3.

In selected cases, fracture surfaces were examined by SEM. Fracture surface area was measured for a number of specimens using an optical stereo-microscope and an image analysis procedure. This allowed to determine reduction of area (RA) values.

Thin-foil samples were prepared for TEM examination by jet-electropolishing using the irradiated discs.

Table 1
Composition of the EM10 (9Cr–1Mo) steel (in wt%)

C	Cr	Mo	V	Nb	Ni	Mn	N	P	Si
0.096	8.8	1.09	–	–	0.18	0.51	0.024	0.015	0.37

Table 2
Irradiation conditions and gas contents for all specimens

Materials	Rod	ID mark	T_1[a] (°C)	T_2[a] (°C)	T_{av}[a] (°C)	dpa	He (appm)	H (appm)
EM10	R1	IE10	275	327	301	11.4	890	4800
tempered	R1	IE3	235	280	257.5	9.8	750	4070
	R1	IE6	181	216	198.5	7.6	570	3110
	R1	IE14	126	150	138	5.4	390	2140
	R10	IE15	178	209	193.5	5.7	220	1860
	R10	IE4	122	143	132.5	4.1	150	1270
	R1	IE11	275	327	301	11.4	890	4800
	R1	IE20	235	280	257.5	9.8	750	4070
	R10	IE21	178	209	193.5	5.7	220	1860
	R10	IE7	178	209	193.5	5.7	220	1860
	R10	IE5	122	143	132.5	4.1	150	1270
	R1	IE[1]*	102	121	111.5	3.9	270	1490
EM10 20%	R1	ID22	280	344	312	12	940	5070
cold-worked	R1	ID13	275	327	301	11.4	890	4800
	R1	ID6	235	280	257.5	9.8	750	4070
	R1	ID3	181	216	198.5	7.6	570	3110
	R1	ID1	126	150	138	5.4	390	2140
	R10	ID17	170	201	185.5	5.7	220	1860
	R10	ID18	178	209	193.5	5.7	220	1860
	R10	ID7	117	137	127	4.1	150	1270
	R1	ID20	280	344	312	12	940	5070
	R1	ID10	275	327	301	11.4	890	4800
	R1	ID[5]*	302	359	330.5	10.6	820	4450
EM10	R1	IF5	247	286	266.5	9.8	750	4070
as-quenched	R1	IF2	129	153	141	5.4	390	2140
	R10	IF16	178	209	193.5	5.7	220	1860
	R10	IF12	125	147	136	4.1	150	1270

Note: The He and and H concentrations in the table are calculated values. He and H measurements have been performed on some samples irradiated in SINQ target-3 [4]. Measured He contents are in relatively good agreement with calculation results. However, measured H concentrations, depending on irradiation temperature, can be much lower than the calculated values.

*: ID marks with a number in superscript indicate 3 mm discs used for TEM investigations.

[a] T_1: Irradiation temperature during the first 13 months. T_2: irradiation temperature during the last 2 months. T_{av}: 'average' irradiation temperature defined as $T_{av} = (T_1 + T_2)/2$.

TEM observations were performed using a Philips EM430 microscope operated at 300 kV and a Jeol 2010F microscope operated at 200 kV.

3. Results

3.1. Tensile tests

Selected engineering tensile curves for the different irradiated materials are shown on Figs. 1–4 and the tensile properties as a function of irradiation dose are given in Table 3 and plotted in Figs. 5–8. Although the temperature and gas content ranges for the different data points are rather large, some trends can be observed in the evolution of the tensile properties with dose. The tempered and cold-worked materials displayed similar behaviours (Figs. 5–7). A drastic decrease in uniform elongation is seen already for the lowest available dose in our set of irradiated specimens and the UE value remains approximately constant up to 10 dpa. Over this dose range, following an initial drop, the total elongation stays rather constant at a value above 4%, while there is a large increase in yield stress and ultimate tensile strength. For the few data points corresponding to doses higher than 10 dpa, there is a sudden change of behaviour: a 'recovery' of the strain-hardening capacity of the irradiated materials takes place, associated with an increase in uniform elongation to more than 4%. The total elongation increases likewise. It must be pointed out that although their tensile properties have not been plotted, two cold-worked specimens irradiated to more than 10 dpa, specimens ID20 and ID10 (cf. Table 2), were tested at 350 and 250 °C, respectively. In both cases, a similar 'recovery' phenomenon was observed.

As-quenched EM10 displayed a different radiation response, as shown on Figs. 4 and 8. The most striking feature is that irrespective of dose and irradiation

Table 3
Tensile properties

Materials	ID mark	dpa	YS (MPa)	UTS (MPa)	UE (%)	TE (%)	RA (%)	T_{test} (°C)
EM10 tempered	–	0	603	761	7.5	14.8	68	25
	–	0	552	657	4.4	10.6	57.5	250
	IE10	11.4	1071	1127	8.2	14.8	–	25
	IE3	9.8	1151	1167	0.5	5.9	50	25
	IE6	7.6	1039	1060	0.7	6.6	59	25
	IE14	5.4	1054	1060	0.4	6.4	59	25
	IE15	5.7	946	993	0.85	9.4	59.5	25
	IE4	4.1	930	966	0.8	6.5	–	25
	IE20	9.8	952	962	0.8	4.9	46.5	250
	IE21	5.7	991	1016	0.7	7.1	58	250
	IE7	5.7	1096	1137	2.4	7.1	57	250
	IE5	4.1	1002	1042	0.95	5.4	–	250
	IE11	11.4	851	915	4.8	9.0	–	350
EM10 20% cold-worked	–	0	809	847	0.7	7.2	63	25
	–	0	797	807	0.4	5.7	–	250
	ID22	12	1181	1189	3.4	7.5	–	25
	ID13	11.4	1151	1180	4.5	10.95	–	25
	ID6	9.8	1226	1240	0.5	5.2	44	25
	ID3	7.6	1090	1126	1.2	4.9	–	25
	ID1	5.4	1093	1093	0.2	5.1	–	25
	ID17	5.7	1045	1054	0.4	4.9	–	25
	ID18	5.7	1073	1083	0.45	5.7	–	25
	ID7	4.1	1249	1311	0.75	5.7	65.5	25
	ID10	11.4	989	1023	2.7	7.7	–	250
	ID20	12	920	963	2.4	6.3	–	350
EM10 as-quenched	–	0	943	1297	5.4	12.3	56	25
	IF5	9.8	1319	1340	0.45	0.75	2	25
	IF2	5.4	1122	1122	0	0	–	25
	IF16	5.7	1178	1178	0	0	–	25
	IF12	4.1	1402	1409	0.2	0.3	–	25

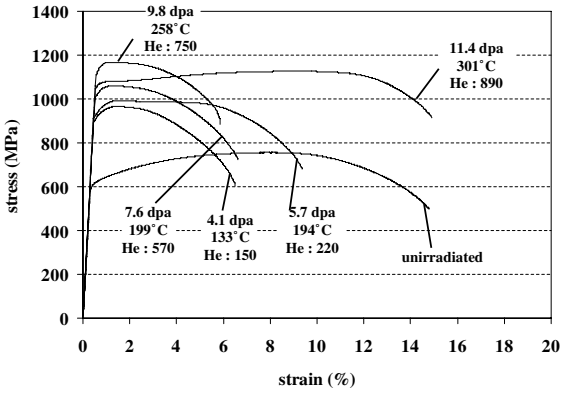

Fig. 1. Selected engineering tensile curves for tempered EM10, tested at room temperature. For each curve, the irradiation dose is indicated, together with the average irradiation temperature (as defined in Table 2) and the helium concentration in appm.

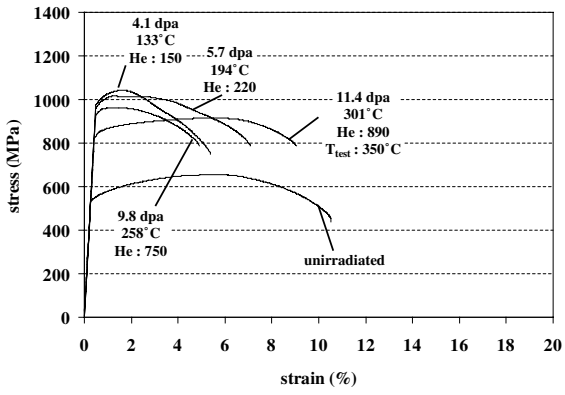

Fig. 2. Selected engineering tensile curves for tempered EM10, tested at 250 °C except for one curve corresponding to a test carried out at 350 °C. As in Fig. 1, irradiation dose, average irradiation temperature and helium concentrations are indicated.

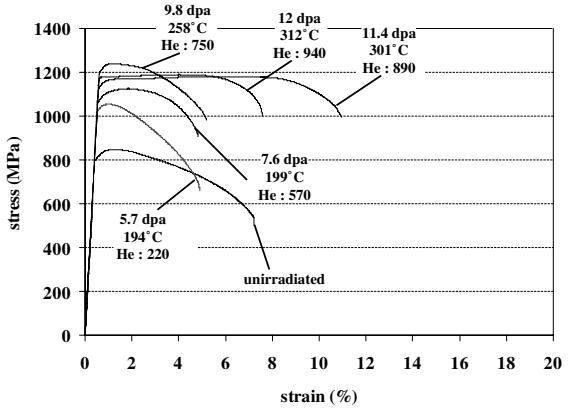

Fig. 3. Selected engineering tensile curves for 20% cold-worked EM10, tested at room temperature. As in Fig. 1, irradiation dose, average irradiation temperature and helium concentrations are indicated.

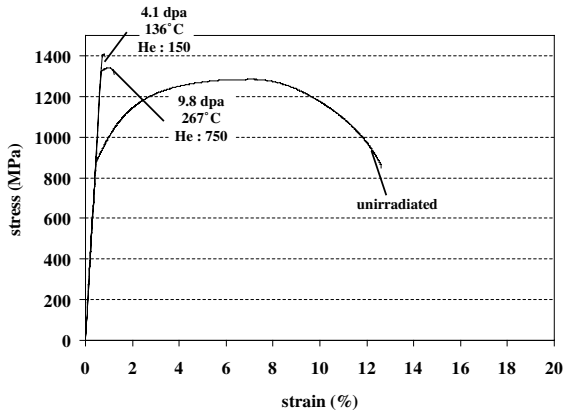

Fig. 4. Selected engineering tensile curves for as-quenched EM10, tested at room temperature. As in Fig. 1, irradiation dose, average irradiation temperature and helium concentrations are indicated.

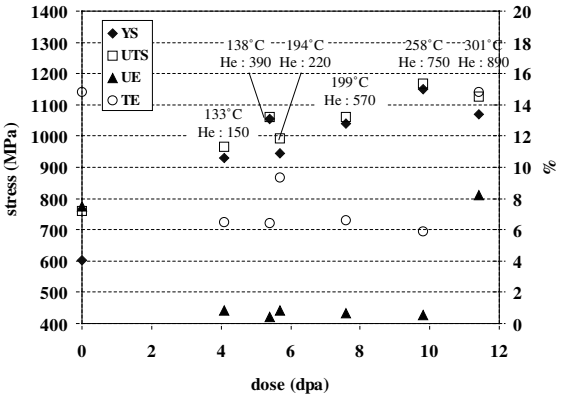

Fig. 5. Evolution of the yield stress at 0.2% plastic strain (YS), ultimate tensile strength, (UTS), uniform and total elongations (UE, TE) as a function of dose, for tempered EM10 specimens tested at room temperature. Average irradiation temperatures and helium concentrations are indicated.

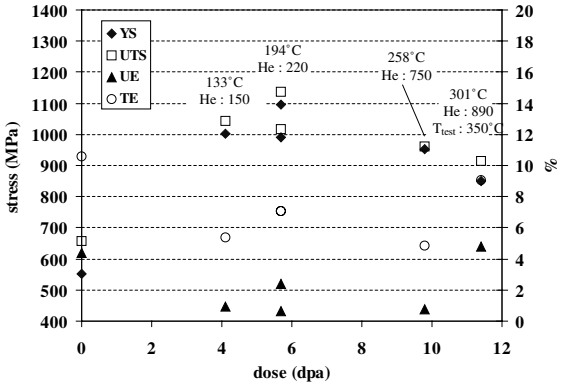

Fig. 6. Evolution of the yield stress at 0.2% plastic strain (YS), ultimate tensile strength, (UTS), uniform and total elongations (UE, TE) as a function of dose for tempered EM10 specimens tested at 250 °C, except where noted. Average irradiation temperatures and helium concentrations are indicated.

temperature, all tested specimens displayed hardly any plastic deformation. In fact, two of them broke at yield and the other two broke clearly in the elastic regime. The irradiated specimens reached high strengths, up to 1400 MPa.

RA values measured on selected broken specimens are presented on Fig. 9. There is a gradual decrease of reduction of area with dose for the tempered and cold-worked specimens. In the case of the as-quenched specimen, the RA value is close to nil.

3.2. SEM

The fracture surfaces of four specimens irradiated to 9.8 dpa were studied using SEM. Fig. 10 presents the fracture surface of irradiated tempered EM10 together with that of an unirradiated control specimen. The unirradiated specimen displays a fully ductile, transgranular fracture surface (Fig. 10(b)). Numerous secondary cracks can be observed on the fracture surface of the irradiated specimen (Fig. 10(c)) which are absent on that of the unirradiated sample (Fig. 10(a)). The fracture appearance is ductile (Fig. 10(d)) but with poorly defined dimples, which are moreover flat and shallow indicating reduced ductility compared to the unirradiated case. For the unirradiated and irradiated tempered EM10 tested at 250 °C, fracture appearances are very similar to those described above. The fracture surface of the irradiated specimen displays flat dimples (Fig. 11(b)) as well as secondary cracks. However, the secondary

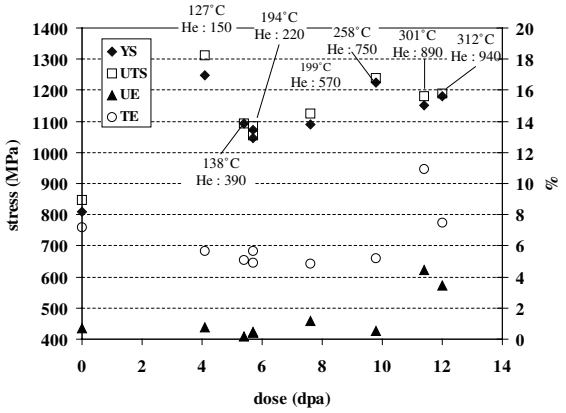

Fig. 7. Evolution of the yield stress at 0.2% plastic strain (YS), ultimate tensile strength, (UTS), uniform and total elongations (UE, TE) as a function of dose, for 20% cold-worked EM10 specimens tested at room temperature. Average irradiation temperatures and helium concentrations are indicated.

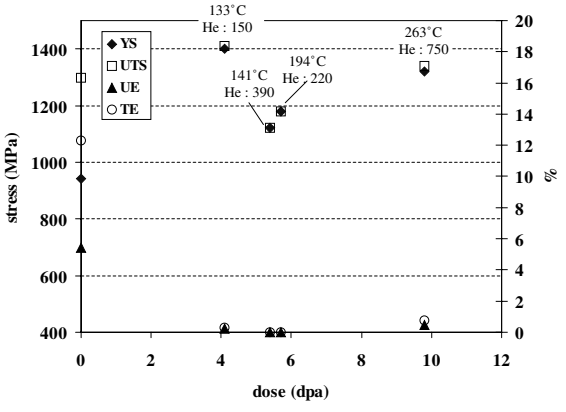

Fig. 8. Evolution of the yield stress at 0.2% plastic strain (YS), ultimate tensile strength, (UTS), uniform and total elongations (UE, TE) as a function of dose, for as-quenched EM10 specimens tested at room temperature. Average irradiation temperatures and helium concentrations are indicated.

crack density is lower than on Fig. 10(c) and the cracks are restricted to the centre of the broken specimen (Fig. 11(a)). The fracture surface of the irradiated 20% cold-worked specimen is covered with secondary cracks Fig. 12(a), some of which seem to outline grain boundaries (Fig. 12(d)). The fracture appearance is predominantly ductile (Fig. 12(b)) but some rare cleavage zones are also found (Fig. 12(c)). The fracture surface of the unirradiated cold-worked specimen is similar to that shown on Fig. 10(b), i.e. fully ductile.

The fracture mode for the unirradiated as-quenched specimen (Fig. 13(b)) is clearly fully ductile as shown by the well defined dimples. A complete change of fracture

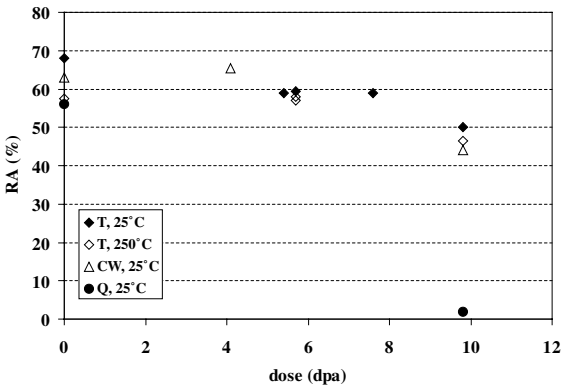

Fig. 9. Graph showing reduction of area vs. dose for tempered (*T*), 20% cold-worked (CW) and as-quenched EM10, tested either at 25 or 250 °C.

mode is observed for the irradiated specimen. Fig. 13(c) shows that no necking took place before fracture. Moreover, the fracture surface, which lies strictly perpendicular to the specimen axis (Fig. 13(c)), displays a fully brittle, intergranular appearance (Fig. 13(d)). There are also some cleavage zones (Fig. 13(e)) particularly in the outer part of the fracture surface.

3.3. TEM

Preliminary TEM investigations were performed on two 3 mm discs irradiated in Rod 1 (cf. Table 2): the first one was a cold-worked sample irradiated to 10.6 dpa at 330 °C, the second one was in the tempered condition and irradiated to 3.9 dpa at about 110 °C. Representative irradiation-induced microstructures are shown on Fig. 14(a) and (b) for the cold-worked and tempered specimen, respectively. In both cases points defects clusters are present in the form of black dots as well as clearly resolved dislocation loops, some of which are larger than 20 nm in diameter. Also, particularly in the case of the cold-worked specimen, signs of dislocation climb are seen as well as interactions between dislocation lines and loops. Furthermore, small bubbles, presumably filled with helium were detected in the cold-worked specimen as shown on Fig. 15. We did not attempt to determine the bubble number density nor the size distribution. A rough estimate of the average diameter is about 2 nm.

4. Discussion

In the following we will first focus on the results obtained on as-quenched EM10 martensitic steel and compare them to earlier data relative to the same material irradiated in a fission reactor. In a second part, the

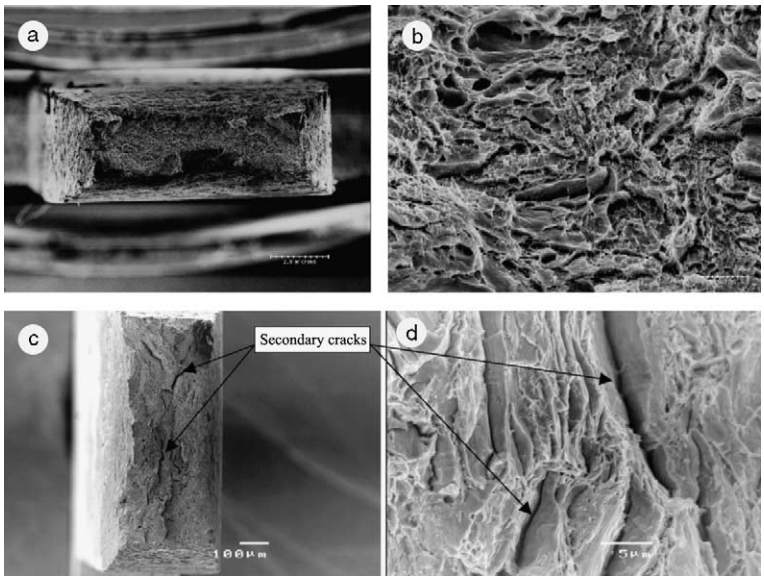

Fig. 10. SEM micrographs showing the fracture surfaces of tempered EM10 specimens tested at room temperature. (a) and (b): Unirradiated control specimen, (c) and (d): specimen irradiated to 9.8 dpa (IE3, cf. Table 2).

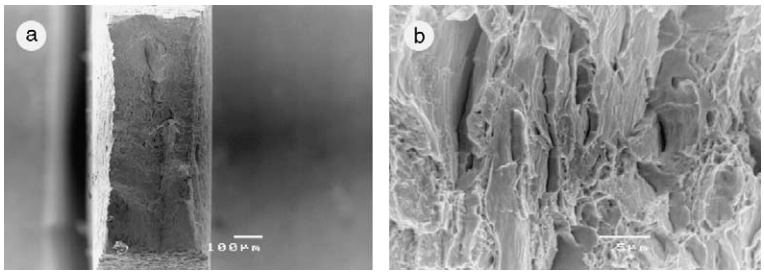

Fig. 11. SEM micrographs showing the fracture surfaces of a tempered EM10 specimen irradiated to 9.8 dpa and tested at 250 °C (IE20, cf. Table 2).

tensile properties measured on tempered EM10 will be discussed and compared to data obtained both in fission and spallation environments.

Although martensitic steels are always used following a temper treatment, the study of irradiation-induced effects in as-quenched martensitic steels is interesting as a contribution to basic knowledge concerning radiation effects in materials. Therefore, as-quenched EM10 tensile specimens were included in an irradiation experiment carried out in the mixed-spectrum nuclear reactor Osiris [6,7]. The specimens were irradiated at 325 °C to different doses, from 0.8 to 9 dpa. Tests were conducted either at room temperature or at 325 °C. It must be emphasised that the same EM10 heat was used for both irradiations in SINQ and Osiris.

It is interesting to compare the effects of the two radiation environments on the tensile properties, even though there are differences in the irradiation temperatures. Figs. 16 and 17 present the evolution with dose of the yield stress and total elongation, respectively, for as-quenched EM10 tensile specimens irradiated either in the Osiris reactor or in SINQ target-3. One can see that fission neutron irradiation induces increases in strength even larger than those observed following irradiation in a spallation environment. Nevertheless, the Osiris irradiated specimens still retain some ductility as shown by the total elongation values whereas the SINQ-irradiated specimens display a complete loss of ductility.

Moreover, the reduction of area is a relevant parameter for assessing the ductility of steels. For instance, it has been established for thermally aged and neutron-irradiated martensitic steels that there is a correlation between reduction of area and the upper shelf energy determined from Charpy impact tests [6,8]. RA values for as-quenched specimens irradiated in Osiris and SINQ are plotted in Fig. 18. There is very little variation of reduction of area for the neutron-irradiated specimens.

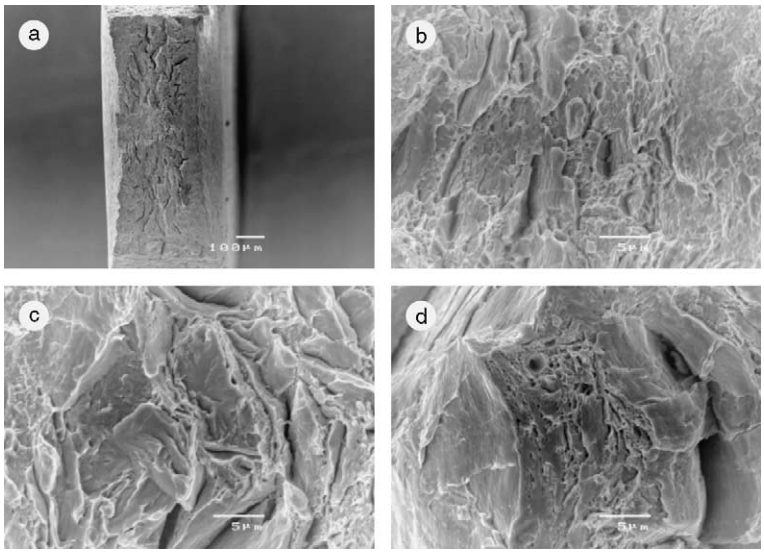

Fig. 12. SEM micrographs showing the fracture surfaces of a 20% cold-worked specimen irradiated to 9.8 dpa and tested at room temperature (ID6, cf. Table 2).

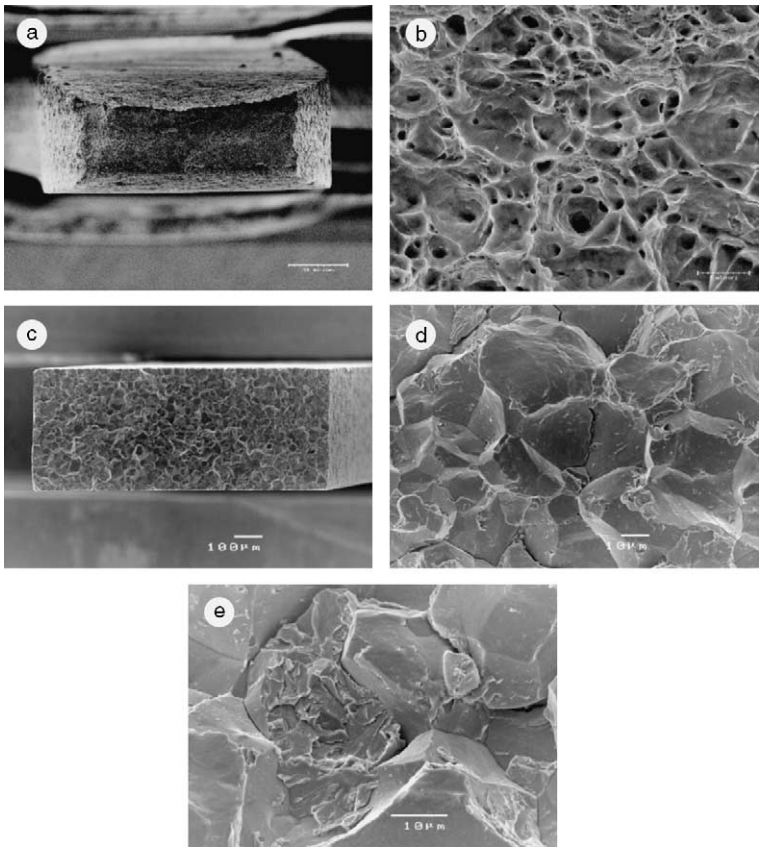

Fig. 13. SEM micrographs showing the fracture surfaces of as-quenched EM10 specimens tested at room temperature. (a) and (b): Unirradiated control specimen, (c), (d) and (e): specimen irradiated to 9.8 dpa (IF5, cf. Table 2).

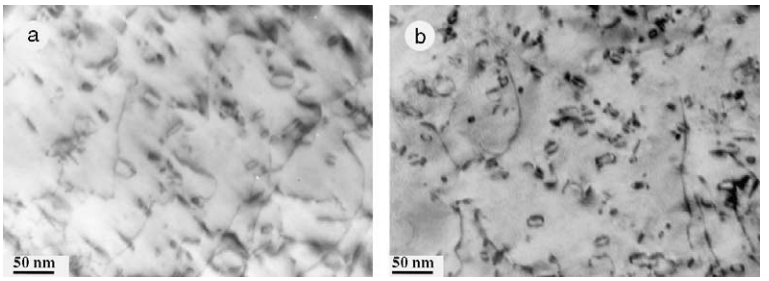

Fig. 14. TEM micrograph showing the irradiation-induced defect microstructure in (a) cold-worked EM10 irradiated at 330 °C to 10.6 dpa, (b) tempered EM10 irradiated at 111 °C to 3.9 dpa.

Fig. 15. TEM micrograph showing small bubbles in cold-worked EM10 irradiated at 330 °C to 10.6 dpa. Under-focus imaging conditions ($\delta f = -1000$ nm). The scale bar represents 10 nm.

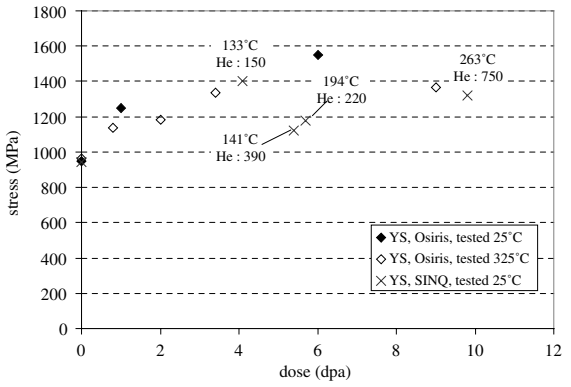

Fig. 16. Evolution of yield stress vs. dose for as-quenched EM10 tensile specimens irradiated either in SINQ target-3 (average irradiation temperatures and helium concentrations are indicated) or in the Osiris reactor [6,7].

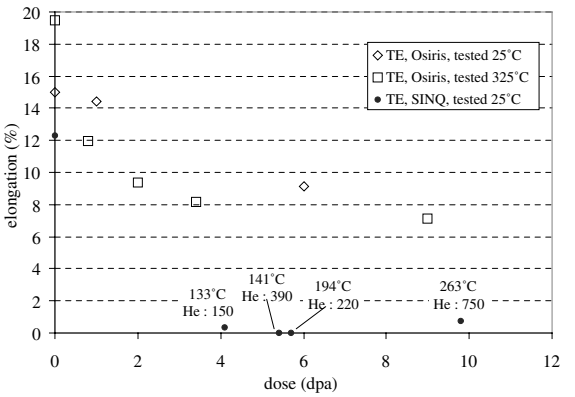

Fig. 17. Evolution of total elongation vs. dose for as-quenched EM10 tensile specimens irradiated either in SINQ target-3 or (average irradiation temperatures and helium concentrations are indicated) or in the Osiris reactor [6,7].

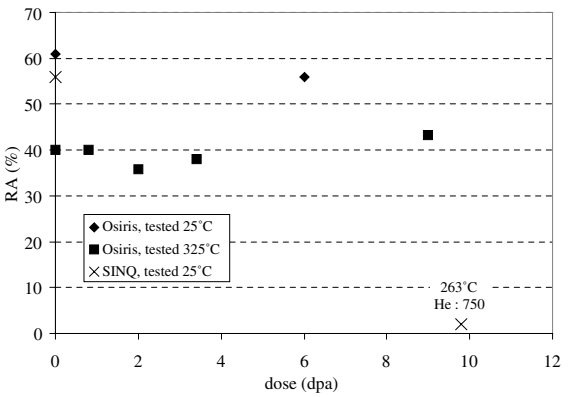

Fig. 18. Graph showing reduction of area vs. dose for as-quenched EM10 tensile specimens irradiated either in SINQ target-3 (average irradiation temperatures and helium concentrations are indicated) or in the Osiris reactor [6,7]. Test temperature is indicated.

The sample irradiated in SINQ to 9 dpa is fully brittle, with no reduction of area at failure, as expected in the case of an intergranular failure mode (cf. Fig. 13). Moreover, the specimens irradiated to lower doses, broke either at yield or in the elastic part of the tensile test. Although no fracture surface measurement nor any SEM investigation were performed on these specimens, it is reasonable to assume that they also failed in an intergranular manner.

Such a totally brittle intergranular failure mode was also observed for EM10 and T91 (mod. 9Cr–1Mo martensitic steel) implanted at 250 °C with helium to concentrations higher than 2500 appm [9]. It is suggested that this failure mode results from the combined effects of a very high implantation-induced hardening and grain boundary weakening due to helium [10] which was shown to greatly reduce grain boundary cohesion in iron [11] and nickel [12]. A similar mechanism could be operative here. However, calculated helium contents in the as-quenched specimens tested in the present work are significantly lower than 2500 appm (cf. Table 2). Helium may not be the only element contributing to intergranular failure. Hydrogen is generated in the irradiated as-quenched specimens to concentrations as high as 4000 appm. This element is well known for its embrittling effects. It has been shown [13] for instance that electrochemical loading of pre-irradiated 9Cr–2W steel tensile specimens causes strong embrittlement. Of course, unlike helium, a substantial amount of the produced hydrogen is not retained but diffuses out of the specimens. Hydrogen measurements recently performed using F82H (a 8% Cr martensitic steel) samples irradiated in SINQ target-3 [4] have shown that for irradiation temperatures lower than 200 °C, the ratio of the measured hydrogen content to the produced quantity was above 30%, while this ratio dropped to about 10% for a sample irradiated at 295 °C. This would suggest that at least for specimens IF2 and IF16, the retained hydrogen content was above the critical concentration for hydrogen embrittlement (≈10 wt ppm) in 9–12% Cr stainless steels [14]. It must be mentioned, however, that the mechanism suggested above fails to explain all our experimental results. For instance, intergranular failure mode was not observed in the case of cold-worked EM10, although irradiation-induced strength levels for this material are close to those measured on as-quenched EM10 following irradiation.

Concerning the tensile properties of tempered martensitic steels irradiated in a spallation environment, experimental results were previously reported by a number of authors, in particular Maloy et al. [3], Farrell and Byun [2] and Dai et al. [15]. The materials involved in these experiments were mod. 9Cr–1Mo [2,3], low activation 9Cr–2W VTa steel [2] as well as DIN 1.4926, a 11.5% Cr steel [15], all in the normalised and tempered metallurgical conditions. Their irradiation temperatures were somewhat lower than those of the specimens irradiated in SINQ target-3. The samples tested by Maloy et al. and by Farrell and Byun had been irradiated at LANSCE with 800 MeV protons and spallation neutrons at temperatures ranging from 50 to 160 °C to a maximum dose of about 10 dpa. Dai et al. performed tests on tensile specimens cut from a beam window irradiated at LANSCE, whose maximum temperature was about 230 °C. The dose range for the specimens was 0.3–6.6 dpa.

The results obtained in the above-mentioned experiments are qualitatively similar to those reported here as regards tempered EM10, at least for doses lower than 10 dpa. A sharp increase of yield strength with dose is observed, together with a drastic decrease of the uniform elongation to less than 1% after exposure to no more than a few tenth of dpa.

Tempered EM10 samples had also been included in the irradiation experiment mentioned above, which was conducted in the Osiris reactor. The increase in yield stress with respect to the yield stress of virgin samples is plotted in Fig. 19 as a function of dose for tempered EM10 samples irradiated either in SINQ target-3 or in Osiris. Farrell and Byun's data [2] for mod. 9Cr–1Mo irradiated at LANSCE are also shown. Fig. 20 presents the evolution with dose of the uniform elongation. The decrease in uniform elongation is significantly more rapid for the materials irradiated in a spallation environment than for the specimens irradiated in Osiris. However Farrell and Byun compared their data with earlier results obtained for the same steels irradiated at 50 °C in the fission reactor HFIR [2] and observed an identical behaviour as regards the uniform elongation

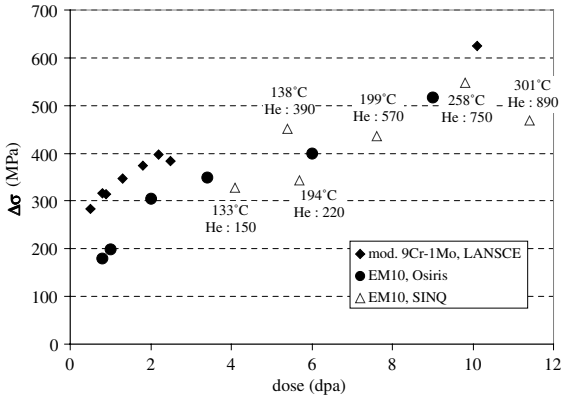

Fig. 19. Evolution of the yield stress increase $\Delta\sigma$ as a function of dose. Triangles: tempered EM10 irradiated in SINQ target-3 (average irradiation temperatures and helium concentrations are indicated). Dots: tempered EM10 irradiated in the Osiris reactor [6,7]. Diamonds: tempered mod. 9Cr–1Mo irradiated at LANSCE [2]. The tensile tests were performed at room temperature.

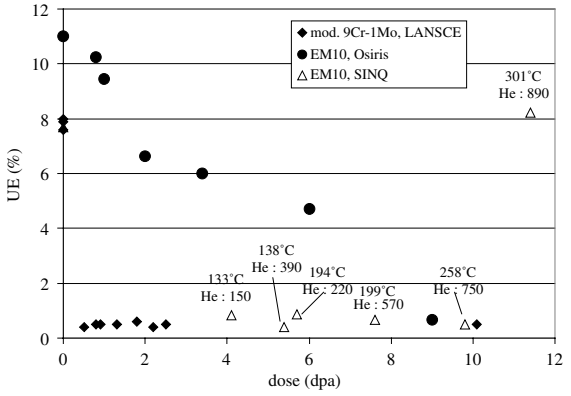

Fig. 20. Evolution of the uniform elongation as a function of dose. Triangles: tempered EM10 irradiated in SINQ target-3 (average irradiation temperatures and helium concentrations are indicated). Dots: tempered EM10 irradiated in the Osiris reactor [6,7]. Diamonds: tempered mod. 9Cr–1Mo irradiated at LANSCE [2]. The tensile tests were performed at room temperature.

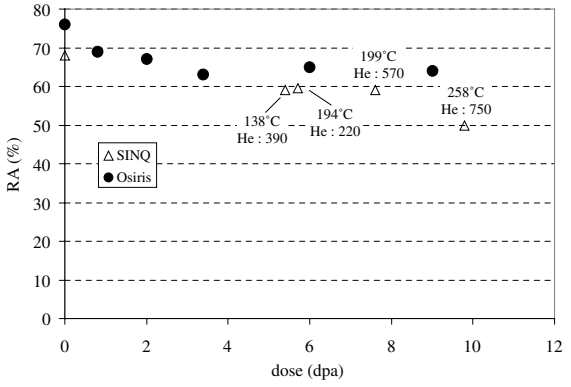

Fig. 21. Evolution of the reduction of area as a function of dose. Triangles: tempered EM10 irradiated in SINQ target-3 (average irradiation temperatures and helium concentrations are indicated). Dots: tempered EM10 irradiated in the Osiris reactor [6,7]. The tensile tests were performed at room temperature.

decrease rate. This tends to indicate that the slower decrease of uniform elongation for the EM10 specimens irradiated in Osiris does not result from a difference in radiation spectrum. The higher irradiation temperature in Osiris (325 °C as already mentioned) could partly explain the slower decrease. However, it must be pointed out that for F82H and Manet-II (a 10.5% Cr martensitic steel) which had also been included in the Osiris irradiation, the uniform elongation was found to decrease more rapidly with dose than in the case of EM10 irradiated in the same conditions [6,16].

Up to about 10 dpa, the yield stress evolution as a function of dose is similar for tempered EM10 irradiated in fission or spallation environments. The same is true as concerns the reduction of area as shown on Fig. 21 with perhaps the exception of the specimen irradiated to 9.8 dpa which displays slightly more embrittlement. Farrell and Byun however, observed that both 9Cr steels irradiated to 10 dpa at LANSCE were markedly stronger than extrapolations of the HFIR data would indicate and suggested that this might be a result of the much larger gas contents. This trend is not seen in the present work. On the contrary, for the specimens irradiated at doses higher than 10 dpa, there is a decrease of yield stress and a sudden 'recovery' of ductility. This phenomenon occurs not only for tempered EM10 tested at room temperature but also for this material tested at 250 °C as well as for cold-worked EM10 tested either at room temperature, 250 or 350 °C as mentioned in Section 3.1. To our knowledge, there are no published data relative to the tensile properties of martensitic steels irradiated with fission neutrons to doses higher than 10 dpa at temperatures in the range 300–350 °C. However, impact properties were measured for the Manet-I martensitic 10.6% Cr steel irradiated to exposure doses of 5–15 dpa at about 300 °C [17]. The results do not indicate any 'recovery' phenomenon at doses higher than 10 dpa.

The informations obtained from the preliminary TEM examinations performed on irradiated discs show that the defect microstructures in both cold-worked EM10 irradiated at 330 °C to 10.6 dpa (sample ID[5], see Table 2) and tempered EM10 irradiated at 111 °C to 3.9 dpa (IE[1] sample) consists of black dots and dislocation loops, some of which are larger than 20 nm. Schäublin and Victoria [18] observed a very similar microstructure in F82H martensitic steel irradiated with neutrons at 310 °C to 10 dpa, as well as Dai et al. [15] in DIN 1.4926 irradiated at LANSCE to 6.6 dpa at about 230 °C. Jia et al. have recently performed a systematic TEM study on F82H and T91 disc samples irradiated in SINQ target-3 [5,19]. High densities of helium bubbles with sizes greater than approximately 1 nm were observed for irradiation temperatures above 200 °C. Our microstructural observations are consistent with these results. By contrast, helium bubbles could not be detected by Dai et al. in DIN 1.4926 irradiated at LANSCE and, as mentioned above, no 'recovery' of ductility was observed by these authors in the dose range 0.3–6.6 dpa [15].

It is not clear however how the presence of tiny helium bubbles could explain the partial recovery of work-hardening capacity as well as the improved ductility at doses higher than 10 dpa. Loss of work-hardening and uniform elongation which occurs in irradiated steels results from plastic flow localisation. Different deformation mechanisms have been identified, in particular dislocation channeling, i.e. strain localisation in slip-bands with reduced defect density, which was observed

in many materials including a Fe–9Cr type ferritic alloy [20]. Deformation microstructures were recently examined [21] for 316 LN specimens either irradiated to 10 dpa at 200 °C with Fe ions or irradiated with helium ions to 1.5 dpa corresponding to a helium concentration of 2 at.%. The specimens were subsequently strained to 10% by the disk-bend method. The deformation mode was not changed by the presence of a high density of small helium bubbles. In both cases channel bands were observed, indicating plastic flow localisation.

It must be pointed out that the microstructures of the tensile specimens are not actually known since the TEM investigations were performed on separately irradiated discs. In fact all the specimens which displayed a surprising ductility were located next to each-other in the target, in contrast to the 3 mm discs used for the TEM work. As already mentioned, the target was hit by a focused beam and as a result some specimens must have reached high temperatures, which might have induced a modification of the irradiation-induced microstructure (partial annealing of the defect clusters, coarsening of the bubble microstructure?). This remains of course very speculative until the microstructures of the tensile specimens are examined.

5. Conclusions

The tensile properties of 9Cr–1Mo martensitic steel were measured after irradiation in a spallation environment at temperatures ranging from about 130 to over 300 °C. This material was irradiated in the tempered, 20% cold-worked and as-quenched conditions. Radiation responses were different depending on the metallurgical condition. The as-quenched specimens were found to be drastically embrittled by irradiation. They displayed a total loss of ductility and the SEM observations performed on one specimen showed a nearly fully intergranular fracture mode. This behaviour is in contrast to that of the same as-quenched steel irradiated at 325 °C in a fission reactor, which, although very much hardened by irradiation, retained substantial ductility and displayed a fully ductile failure mode. It is believed that the generation of significant amounts of both helium and hydrogen in the specimens irradiated in a spallation spectrum together with the large irradiation-induced hardening of an already very strong material are two important factors leading to the observed tensile behaviour and intergranular fracture mode. The evolution with dose of the tensile properties of the cold-worked and annealed specimens displayed up to about 10 dpa a similar behaviour to that observed by other authors in tempered martensitic steels after irradiations in spallation or fission environments. Radiation hardening increased and uniform elongation decreased with increasing dose, while the decrease in reduction of area was limited. SEM observations of broken specimens showed signs of embrittlement in the irradiated specimens but fracture surface appearances remained on the whole ductile. Preliminary TEM microstructural observations performed on irradiated discs are in good agreement with earlier results. Black dots and large loops were observed in a cold-worked and a tempered specimen irradiated to 10.6 and 3.9 dpa at 330 and 111 °C, respectively and helium bubbles were detected in the specimen irradiated at 330 °C. For the few specimens irradiated to doses higher than 10 dpa, a surprising 'recovery' of ductility is observed. This behaviour might be partly related to a sudden temperature rise of these specimens during the irradiation. TEM investigations of their microstructures are needed before any conclusion is drawn.

Acknowledgements

The authors would like to thank J.-C. Brachet for technical review of the manuscript as well as A. Bougault and V. Rabeau for performing fracture surface examinations and RA measurements on unirradiated tensile specimens. This research was sponsored by the European Union (contract FIKW-CT-2000-00058).

References

[1] Y. Dai, G.S. Bauer, J. Nucl. Mater. 296 (2001) 43.
[2] K. Farrell, T.S. Byun, J. Nucl. Mater. 296 (2001) 129.
[3] S.A. Maloy, M.R. James, G. Willcutt, W.F. Sommer, M. Sokolov, L.L. Snead, M.L. Hamilton, F. Garner, J. Nucl. Mater. 296 (2001) 119.
[4] Y. Dai, Y. Foucher, M. James, B. Oliver, these Proceedings. doi:10.1016/S0022-3115(03)00099-0.
[5] X. Jia, Y. Dai, M. Victoria, J. Nucl. Mater. 305 (2002) 1.
[6] J.C. Brachet, X. Averty, P. Lamagnère, A. Alamo, F. Rosenblum, O. Raquet, J.L. Bertin, in: S.T. Rosinski, M.L. Grossbeck, T.R. Allen, A.S. Kumar (Eds.), Proceedings of the 20th International Symposium on Effects of Radiation on Materials, ASTM STP 1405, ASTM, West Conshohocken, PA, 2001, p. 500.
[7] X. Averty, J.P. Pizzanelli, O. Rabouille, J.J. Espinas, J.C. Brachet, to be published.
[8] M.G. Horsten, E.V. Van Osch, D.S. Gelles, M.L. Hamilton, in: M.L. Hamilton, A.S. Kumar, S.T. Rosinski, M.L. Grossbeck (Eds.), Proceedings of the 19th International Symposium on Effects of Radiation on Materials, ASTM STP 1366, ASTM, West Conshohocken, PA, 2000, p. 579.
[9] P. Jung, J. Henry, J. Chen, J.-C. Brachet, these Proceedings. doi:10.1016/S0022-3115(03)00014-X.
[10] J. Henry, M.-H. Mathon, P. Jung, these Proceedings. doi:10.1016/S0022-3115(03)00118-1.

[11] R. Gupta, to be published.
[12] R.W. Smith, W.T. Geng, C.B. Geller, R. Wu, A.J. Freeman, Scr. Mater. 43 (2000) 957.
[13] A. Kimura, H. Kayano, M. Narui, J. Nucl. Mater. 179–181 (1991) 737.
[14] P. Jung, Fusion Technol. 33 (1998) 63.
[15] Y. Dai, F. Carsughi, W.F. Sommer, G.S. Bauer, H. Ullmaier, J. Nucl. Mater. 276 (2000) 289.
[16] A. Alamo, X. Averty, Fusion Technology, association CEA-EURATOM, annual report 1998.
[17] M. Rieth, B. Dafferner, H.D. Röhrig, C. Wassilew, Fusion Eng. Des. 29 (1995) 365.
[18] R. Schäublin, M. Victoria, J. Nucl. Mater. 283–287 (2000) 339.
[19] X. Jia and Y. Dai, these Proceedings. doi:10.1016/S0022-3115(03)00101-6.
[20] D. Gelles, R. Schäublin, Mater. Sci. Eng. A 309&310 (2001) 82.
[21] E.H. Lee, T.S. Byun, J.D. Hunn, K. Farrell, L.K. Mansur, J. Nucl. Mater. 296 (2001) 183.